SI

Table S1. Pertinent bond lengths (Å) and angles (°) for **3**.

Mn1	Mn2	Mn3	Mn4	Mn5
Mn1-O1 1.928(6)	Mn2-O5 1.925(5)	Mn3-O8 2.104(4)	Mn4-O4 2.424(7)	Mn5-O6 2.272(4)
Mn1-O2 1.910(5)	Mn2-O6 1.912(4)	Mn3-O11 2.11(1)	Mn4-O5 2.114(4)	Mn5-O7' 2.272(4)
Mn1-O3 1.925(6)	Mn2-O7 1.924(5)	Mn3-O13 2.213(6)	Mn4-O12 2.16(1)	Mn5-O14 1.997(5)
Mn1-O4 1.943(5)	Mn2-O8 1.934(4)	Mn3-O15 2.199(8)	Mn4-O13 2.214(5)	Mn5-O14' 1.997(5)
Mn1-O13 2.139(6)	Mn2-O14 2.101(4)	Mn3-O16 2.220(6)	Mn4-O17 2.262(6)	Mn5-O16 2.320(5)
	Mn2-N3 2.336(8)	Mn3-O1 2.577(7)	Mn4-O18 2.219(8)	Mn5-O17 2.290(6)

Mn1	Mn2	Mn3	Mn4	Mn5
Mn1-O4-Mn4 98.8(2)	Mn2-O8-Mn3 113.5(2)	Mn3-O13-Mn1 102.3(2)	Mn4-O5-Mn2 118.6(2)	Mn5-O6-Mn2 97.3(2)
Mn1-O13-Mn4 99.8(2)	Mn2-O5-Mn4 118.6(2)	Mn3-O13-Mn4 128.4(3)	Mn4-O4-Mn1 98.8(2)	Mn5-O7'-Mn2' 97.6(2)
Mn1-O13-Mn3 102.3(2)	Mn2-O14-Mn5 100.6(2)	Mn3-O8-Mn2 113.5(2)	Mn4-O13-Mn1 99.8(2)	Mn5-O14-Mn2 100.6(2)
Mn1-O1-Mn3 96.6(2)	Mn2-O14-Mn5' 101.1(2)	Mn3-O16-Mn5' 104.0(2)	Mn4-O13-Mn3 128.4(3)	Mn5-O14'-Mn2' 101.1(2)
	Mn2-O6-Mn5 97.3(2)	Mn3-O1-Mn1 96.6(2)	Mn4-O17-Mn5 107.5(2)	Mn5-O14-Mn5' 97.7(2)
	Mn2-O7-Mn5' 97.6(2)			Mn5-O14'-Mn5' 97.7(2)
				Mn5-O16'-Mn3' 104.0(2)
				Mn5-O17-Mn3 107.5(2)

Table S2. Bond valence sums for Mn1 – Mn5.

metal VBS	d(M-L1)	d(M-L2)	d(M-L3)	d(M-L4)	d(M-L5)	r(0)	beta
Mn1	2.139	1.943	1.925	1.91	1.928	1.76	0.37
M(Ox.State)	2.91083						

metal VBS	d(M-L1)	d(M-L2)	d(M-L3)	d(M-L4)	d(M-L5)	d(M-L6)	r(0)	beta
Mn2	2.336	2.101	1.952	1.934	1.924	1.912	1.76	0.37
M(Ox.State)	3.133752							

metal VBS	d(M-L1)	d(M-L2)	d(M-L3)	d(M-L4)	d(M-L5)	d(M-L6)	r(0)	beta
Mn3	2.104	2.199	2.213	2.22	2.114	2.557	1.79	0.37
M(Ox.State)	1.933054							

metal VBS	d(M-L1)	d(M-L2)	d(M-L3)	d(M-L4)	d(M-L5)	d(M-L6)	r(0)	beta
Mn4	2.424	2.262	2.114	2.219	2.214	2.155	1.79	0.37
M(Ox.State)	1.880517							

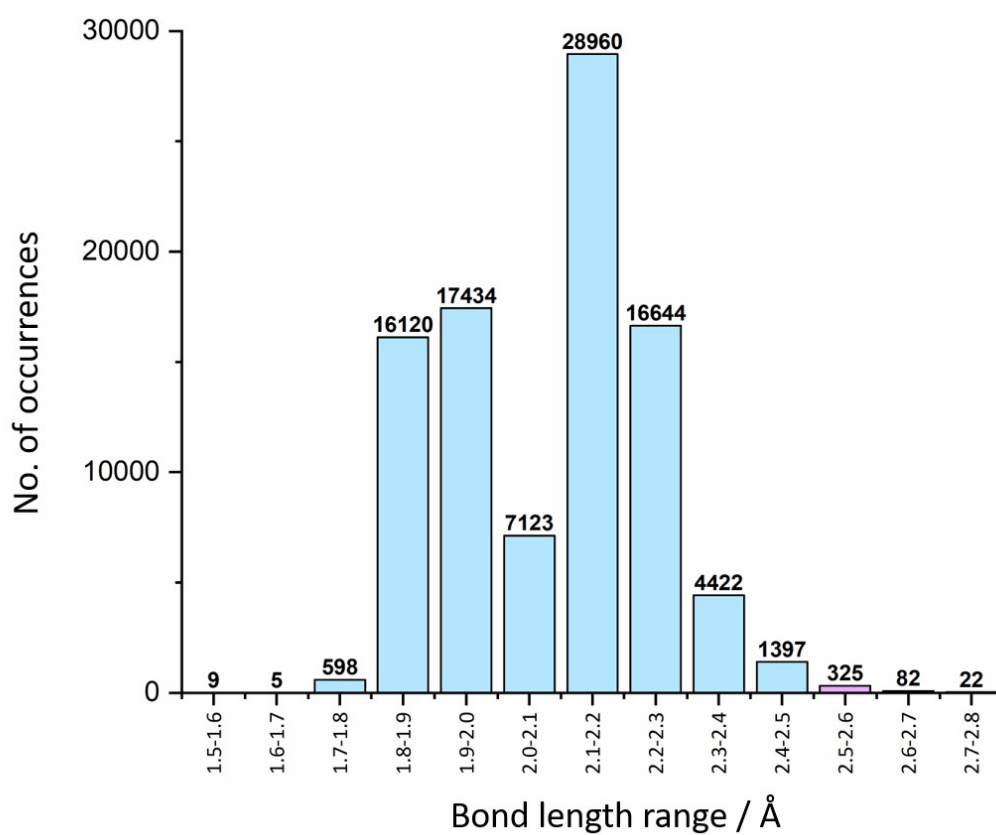| metal VBS	d(M-L1)	d(M-L2)	d(M-L3)	d(M-L4)	d(M-L5)	d(M-L6)	r(0)	beta
Mn5	2.272	2.272	2.29	1.992	1.997	2.32	1.79	0.37
M(Ox.State)	2.192022							

Figure S1. A histogram showing the variation in Mn-O bond lengths in the CSD. The purple bar denotes the range where the Mn3···O1 distance in complex **3** lies.
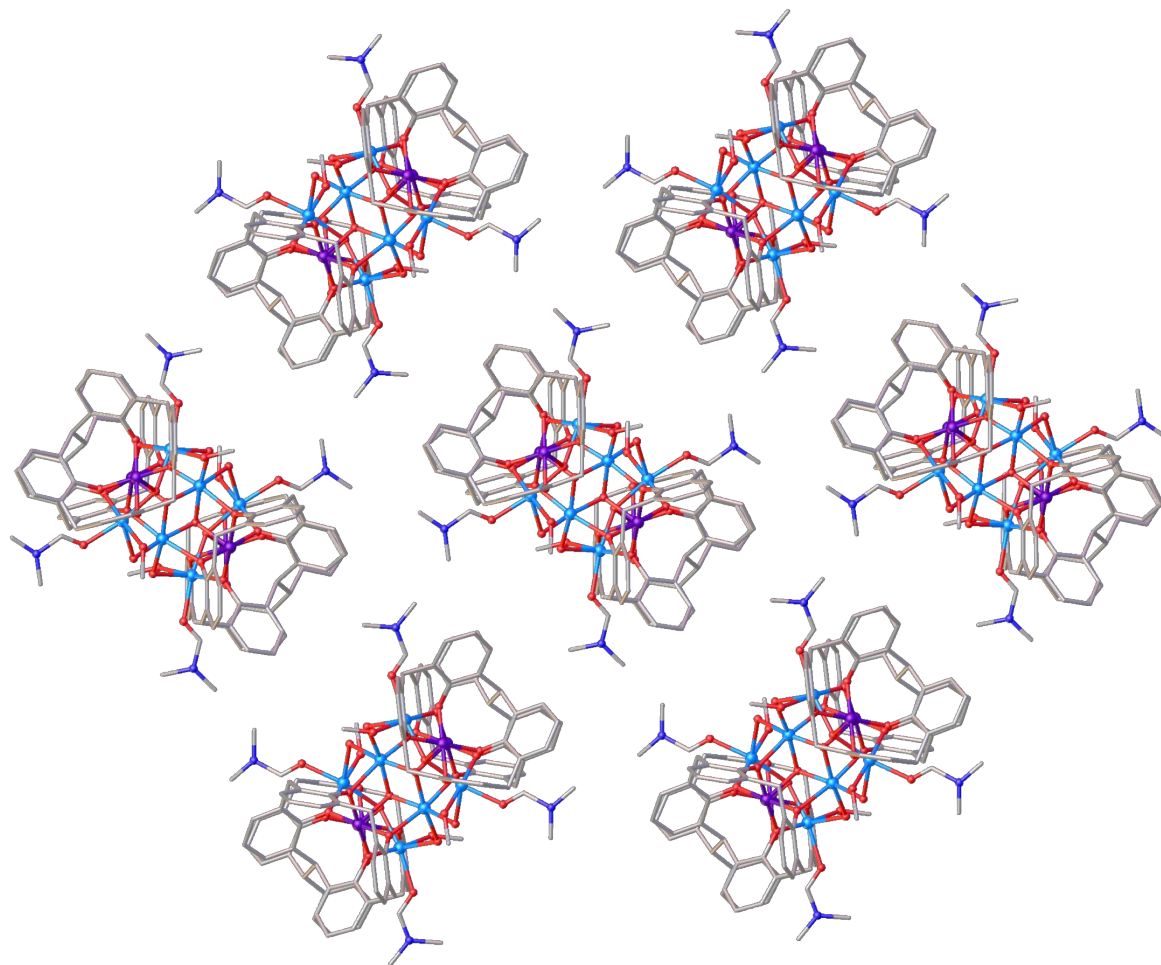
Figure S2. Extended structure of **3** shown along the *a*-axis. The *t*Bu groups of the L ligands, H-atoms, co-crystallised and some ligated solvent are omitted for clarity. Colour code C – grey, O – red, N – dark blue, Mn^{II} – pale blue, Mn^{III} – purple.
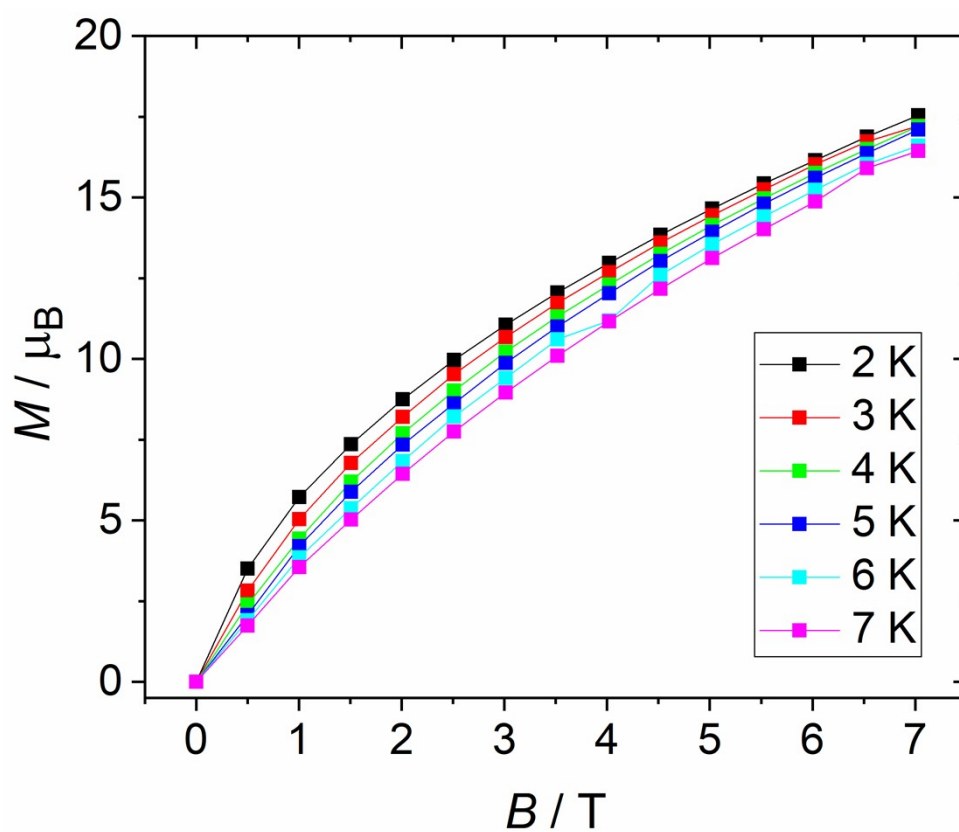
Figure S3. Variable-temperature-variable-field (VTVB) magnetisation data of **3** at T = 2-7 K and B = 0-7 T.

Computational details

DFT calculations were performed on the full crystal structures of complexes **3** and **4**. The energies of each spin configuration were computed using a hybrid UB3LYP functional with the TZV basis set[1] as implemented in Gaussian 16 software. The exchange interactions were estimated using the broken symmetry approach,[2] which has been shown to yield good numerical estimates of J values in polymetallic systems[3] based on the extended pair-wise interaction model, proposed by Ruiz and co-workers.[4] This methodology has been proven to yield very good numerical estimates of exchange interactions for Mn clusters possessing weak ferro/antiferromagnetic coupling.[5] Indeed, there are instances where these calculations were employed to detect errors in experimental susceptibility data due to sample decay.[6] The chosen spin configurations for our calculations are given in Figures S6-S8, along with their corresponding computed spin density plots. The spin-Hamiltonian below was used to estimate the exchange interactions. We have also estimated these using Yamaguchi's spin-projection formula[7] for the model complex, which yielded very similar results (Figure S5).

$E_{HS} = -J_1[\hat{S}_1 \cdot \hat{S}_2] - J_2[\hat{S}_1 \cdot \hat{S}_3 + \hat{S}_1 \cdot \hat{S}_4 + \hat{S}_2 \cdot \hat{S}_5 + \hat{S}_2 \cdot \hat{S}_6] - J_3[\hat{S}_3 \cdot \hat{S}_5 + \hat{S}_4 \cdot \hat{S}_6] - J_4[\hat{S}_3 \cdot \hat{S}_9 + \hat{S}_5 \cdot \hat{S}_9 + \hat{S}_4 \cdot \hat{S}_{10} + \hat{S}_6 \cdot \hat{S}_{10}]$
$- J_5[\hat{S}_1 \cdot \hat{S}_7 + \hat{S}_1 \cdot \hat{S}_8 + \hat{S}_2 \cdot \hat{S}_7 + \hat{S}_2 \cdot \hat{S}_8] - J_6[\hat{S}_3 \cdot \hat{S}_7 + \hat{S}_4 \cdot \hat{S}_8 + \hat{S}_5 \cdot \hat{S}_7 + \hat{S}_6 \cdot \hat{S}_8]$
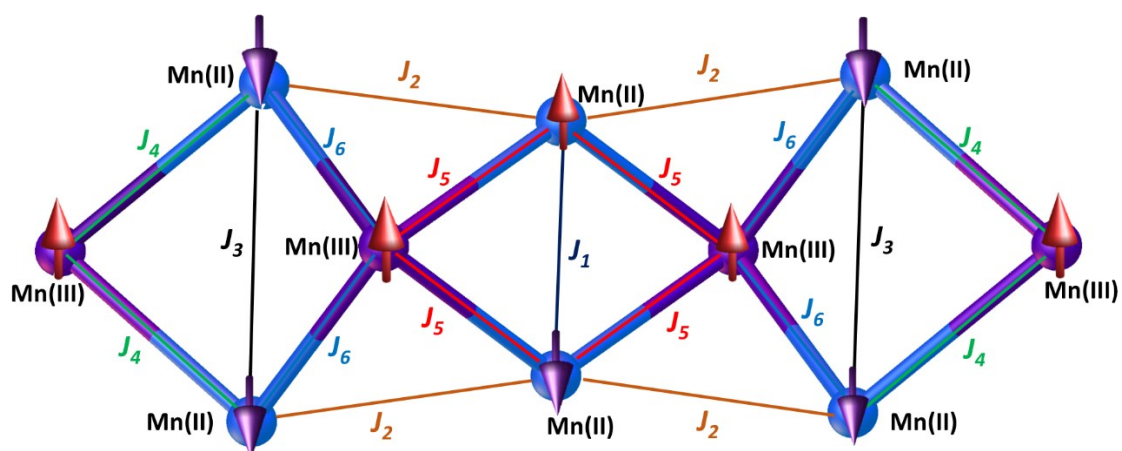

Figure S4. Depiction of the ground state of the complex **3** based on the DFT calculated exchange coupling constants, J_{1-6}.
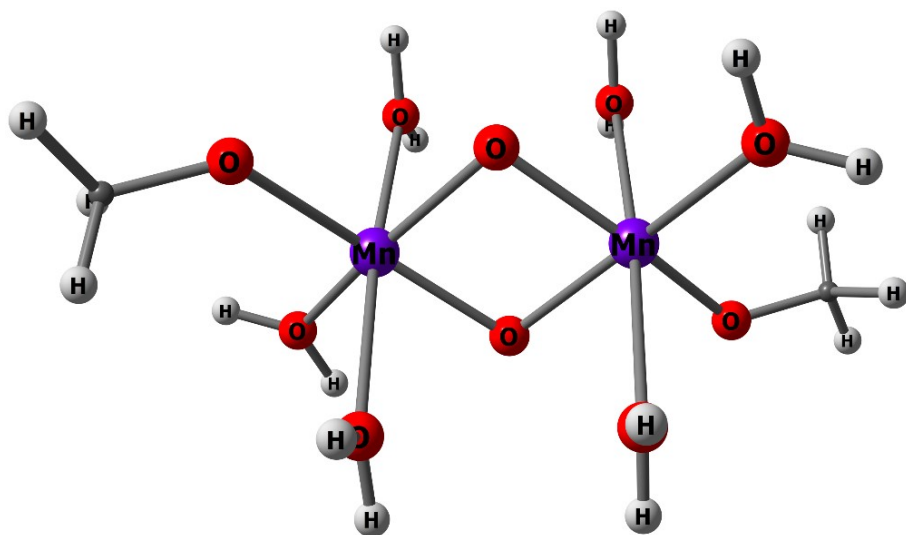

Figure S5. Dimeric model complex taken from the X-ray structure employed to verify the magnitude of J_1 in complex **4**. The exchange interaction obtained in dimeric model is J = -92 cm^{-1}. We have verified the J value using the Yamaguchi model, which computes J = -115 cm^{-1}.
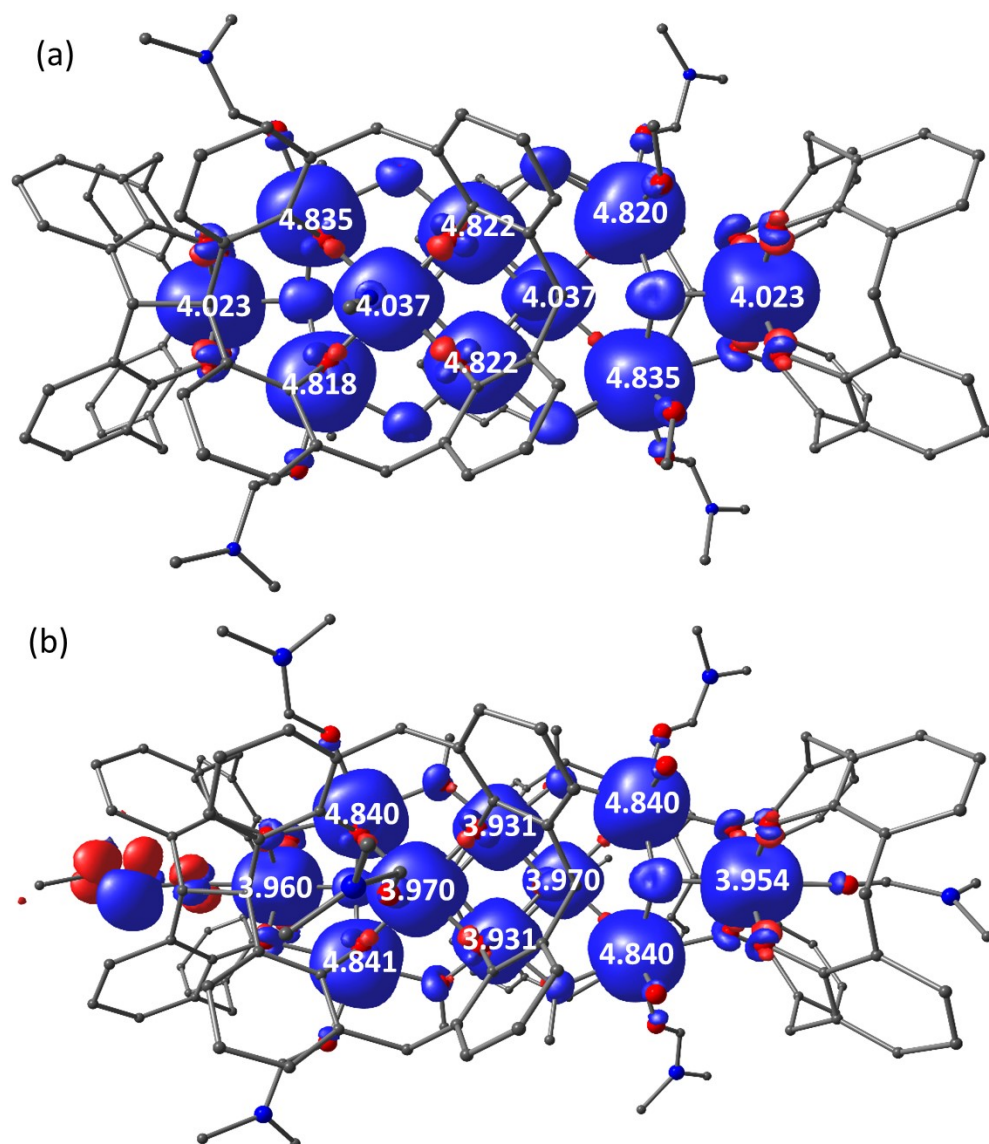
(a)

(b)

Figure S6. Computed spin densities for the high spin state of **3** (a) and **4** (b) with a cut-off value of 0.0006 a.u. The blue colour represents positive spin density and the red colour negative spin density**.**
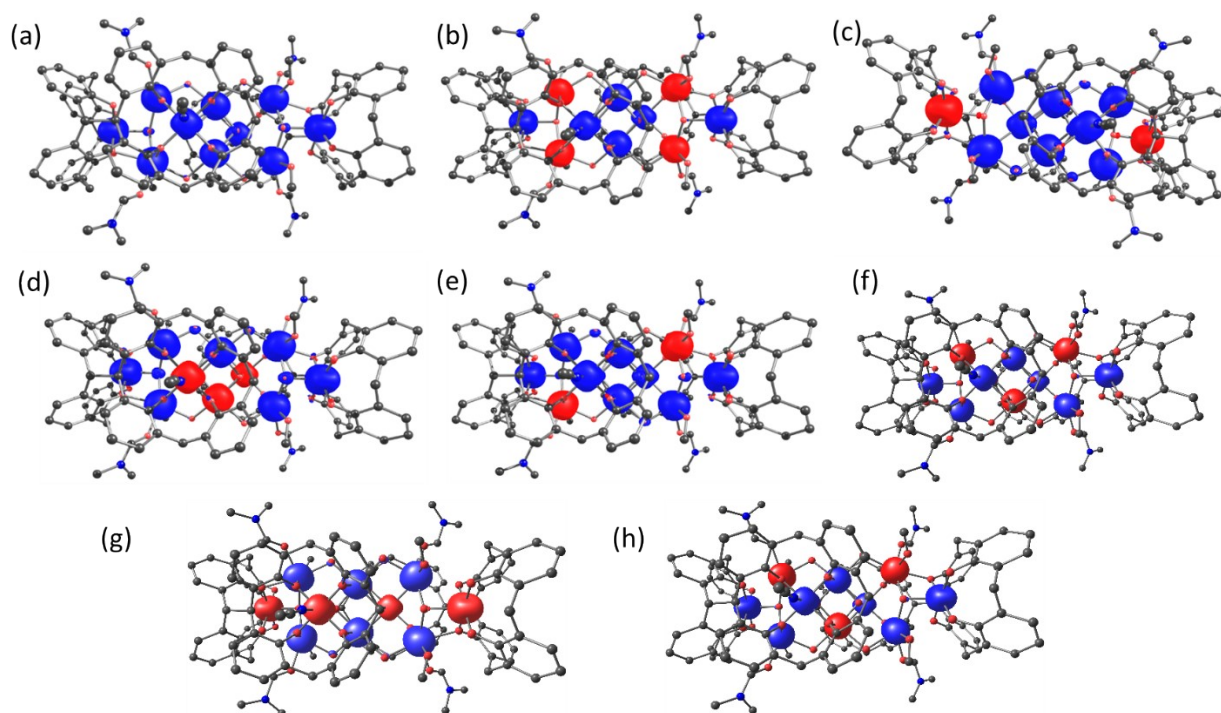
Figure S7. Computed spin density plot for all broken symmetries of complex **3** with a cut-off value of 0.0006 a.u. The blue colour represents positive spin density and the red colour negative spin density**.**

Figure S8. Computed spin density plot for all broken symmetries of complex **4** with a cut-off value of 0.0006 a.u. The blue colour represents positive spin density and the red colour negative spin density**.**
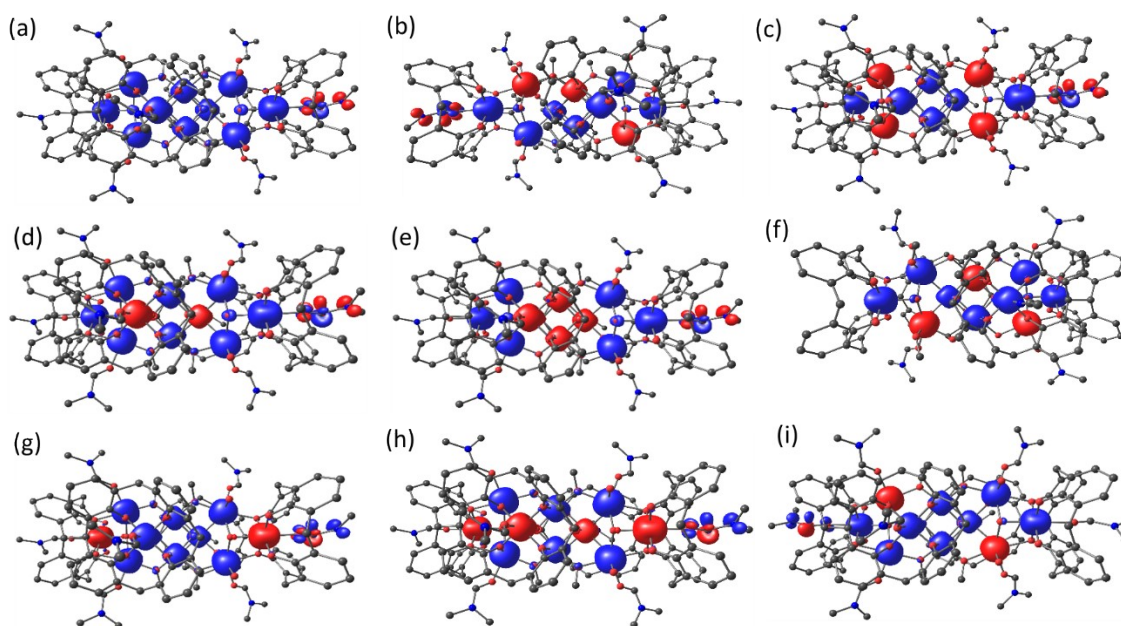
References

1. A. Schäfer, H. Horn and R. Ahlrichs, *J. Chem. Phys*., 1992, **97**, 2571; (b) A. Schäfer, C. Huber and R. Ahlrichs, *J. Chem. Phys*., 1994, **100**, 5829.

2. L. Noodleman, *J. Chem. Phys*., 1981, **74**, 5737– 5743.

3. G. Rajaraman, J. Cano, E. K. Brechin and E. J. L. McInnes, *Chem. Commun*., 2004, 1476–1477; P. Christian, G. Rajaraman, A. Harrison, J. J. W. McDouall, R. E. P. Winpenny, Dalton Trans., 2004, 1511–1512; K. R. Vignesh, S. K. Langley, K. S. Murray and G. Rajaraman, *Chem. Eur. J*., 2015, **21**, 2881–2892; P. Christian, G. Rajaraman, A. Harrison, M. Helliwell, J. J. W. McDouall, J. Raftery and R. E. P. Winpenny, *Dalton Trans*., 2004, 2550–2555.

4. E. Ruiz, A. Rodríguez-Fortea, J. Cano , S. Alvarez and P. Alemany , *J. Comput. Chem*., 2003, **24**, 982-989.

5. a) W. P. Barros, R. Inglis, G. S. Nichol, T. Rajeshkumar, G. Rajaraman, S. Piligkos, H. O. Stumpf and E. K. Brechin, *Dalton Trans*., 2013, **42**, 16510-16517; b) K. R. Vignesh, S. K. Langley, C. J. Gartshore, I. Borilović, C. M. Forsyth, G. Rajaraman and K. S. Murray, *Dalton Trans*., 2018, **47**, 11820–11833; c) K. R. Vignesh, S. K. Langley, C. J. Gartshore, B. Moubaraki, K. S. Murray and G. Rajaraman, *Inorg. Chem*., 2017, **56**, 1932-1949; d) E. Cremades, J. Cano, E. Ruiz, G. Rajaraman, C. J. Milios and E. K. Brechin., *Inorg. Chem*., 2009, **48**, 8012-8019; e) C. J. Milios, M. Manoli, G. Rajaraman, A. Mishra, L. E. Budd, F. White, S. Parsons, W. Wernsdorfer, G. Christou and E. K. Brechin., *Inorg. Chem*., 2006, **45**, 6782-6793.

6. K. R. Vignesh, S. K. Langley, K. S. Murray and G. Rajaraman., *Chem. Eur. J*., 2015, **21**, 2881-2892.

7. T. Onishi, Y. Takano, Y. Kitagawa, T. Kawakami, Y. Yoshioka and K. Yamaguchi, *Polyhedron*, 2001, **20**, 1177.